



HAL
open science

Geometric problems from 3D reflective tomography

Jean-Baptiste Bellet, Gérard Berginc

► **To cite this version:**

Jean-Baptiste Bellet, Gérard Berginc. Geometric problems from 3D reflective tomography. 2018.
hal-01788342

HAL Id: hal-01788342

<https://hal.science/hal-01788342>

Preprint submitted on 9 May 2018

HAL is a multi-disciplinary open access archive for the deposit and dissemination of scientific research documents, whether they are published or not. The documents may come from teaching and research institutions in France or abroad, or from public or private research centers.

L'archive ouverte pluridisciplinaire **HAL**, est destinée au dépôt et à la diffusion de documents scientifiques de niveau recherche, publiés ou non, émanant des établissements d'enseignement et de recherche français ou étrangers, des laboratoires publics ou privés.

GEOMETRIC PROBLEMS FROM 3D REFLECTIVE TOMOGRAPHY

JEAN-BAPTISTE BELLET AND GÉRARD BERGINC

ABSTRACT. Reflective tomography is an emerging method in three-dimensional optical imaging. It empirically extends the domain of validity of X-ray inversion to the visible and near-infrared spectra. In this paper, we show that this extension introduces mathematical challenges, and offers new opportunities in geometry. In the spirit of reflective tomography, we formulate properly new geometrical problems and we derive a heuristics that solves efficiently original problems of geometric tomography. We discuss this heuristics on a canonical case and on numerical results. The argumentation emphasizes the contribution of the singularities, and shows that the method reconstructs especially features, by backprojection of the discontinuities of the input projections. On one side, this shows to opticians that the scope of reflective tomography covers new possibilities, including imaging of active surfaces. On the other side, we address to mathematicians conjectures based on the previous observations, and we suggest approaches to be explored. In a word, this work lays the foundation for further mathematical studies that could upgrade optical applications.

1. INTRODUCTION

1.1. Three-dimensional optical imaging. There is a considerable interest in the development of new optical imaging systems that are able to give three-dimensional images. Potential applications range across the field of defense and security for the recognition of targets, the medical field for the detection of subcutaneous and cutaneous tumors or the archaeological field for the discovery of remains in forests. The framework is the following: given a set of bi-dimensional images in the visible to near-infrared band, construct a three-dimensional model of the original scene. This field is related to several topics.

1.1.1. Radiometry. The first one deals with image formation [19, 24]. This subject, called *radiometry*, is about the modeling of an optical image. In this field, a camera is often modeled as an ideal pinhole, which realizes an ideal perspective projection of the scene [23]; this provides a geometric model of an image by the means of rays of projection. In radiometry the *irradiance* represents the amount of light incident on a surface: it is the power per unit area ($\text{W}\cdot\text{m}^{-2}$) incident on the surface. The *radiance* represents the amount of light radiated from a surface: it is the power per unit area per unit solid angle ($\text{W}\cdot\text{m}^{-2}\cdot\text{sr}^{-1}$). The sensors of a camera measure the (incident) irradiance. Since light is an electromagnetic wave, the Maxwell equations govern its propagation and its behavior at interfaces between media. For a scene of several meters and visible to near-infrared wavelengths ($0.4\mu\text{m}$ - $3\mu\text{m}$), light is often scattered from surfaces, due to subsurface volumic diffusion and due to the rugosity of the surface. The models of radiometry take often this phenomenon into account, by the means of the *Bidirectional Reflectance Distribution Function* (BRDF): the BRDF is a surfacic function defined as the ratio of radiance to irradiance; the incident direction and the radiation direction are arguments of the BRDF. It tells how the surface reflects light toward a radiation direction when it is illuminated from an incident direction. In particular the BRDF can encode the specular reflections on a perfect mirror (Snell-Descartes law); while an ideal matte surface, called a *Lambertian* surface, is encoded by a BRDF which does not depend on the radiation angle. In order to take into account the effects due to the polarization of light, some models go further by using a vectorized version: the interaction of light with a surface is expressed by the means of a Mueller matrix, or a polarimetric BRDF, which acts on a Stokes vector [13, 15, 28]. For a polarized light, incident on a rough surface, some other scattering models are based on the Small Slope Approximation [6, 30].

Date: May 9, 2018.

2000 Mathematics Subject Classification. 78A97, 94A12, 44A12.

Key words and phrases. 3D imaging, computational optics, reconstruction, Radon transform, geometric tomography.

1.1.2. *Reconstruction.* The second main topic deals with inverse problems: reconstruct the 3D scene by combining the 2D projections. In the field of computer vision, this problem is the so-called *multiple-view reconstruction*; standard strategies establish a correspondence of features, such as corners or edges, between the frames; the reconstruction algorithm takes benefit of these correspondences, thanks to linear algebra considerations [23]. Other methods are based on a voxelized 3D reconstruction. In the *shape-from-silhouette* problem, the input images are binary; volumic intersection of the corresponding viewing cones, which is a way of backprojecting the images, reconstructs the *visual hull* of the scene [1, 22]. Some other methods carve iteratively a 3D volume by checking consistency of the input irradiances [21]. In this paper we will discuss *reflective tomography*, which enters also in the class of methods which compute a voxelized reconstruction. And we mention a method which reconstructs a surface and its irradiance by an iterative fitting algorithm [32].

1.1.3. *Tomography.* In transmission tomography, the records are projections containing the X-ray transform of an attenuation; they are processed to provide a reconstruction. The reconstruction method looks like a Radon inversion formula, which is often implemented under the form of a *filtered backprojection* algorithm [25]. This is the basis of tomography, while many variants exist. Exact or heuristic inversion formula dedicated to special geometry of acquisition are derived. For instance the famous FDK algorithm [14] and its refinements such as [33] are heuristic methods dedicated to cone beam (perspective) projections. Also some other imaging modalities are modeled by related transforms; for instance, in emission tomography, the considered transform is an X-ray transform with attenuation [25].

The so-called reflective tomography draws a parallel with transmission tomography: the records are projections with similar geometries. Then the idea is to compute a reconstruction by the means of a filtered backprojection from transmission tomography [20]. This heuristic is successful for several kinds of reflective data [20]; the principle has also been proposed in object modeling from photographs [18]. A recent patented technology is based on 3D reflective tomography [4, 5, 8]; it can reconstruct surfaces from 2D optical images [9–11], and it recovers partially occluded objects [7].

1.1.4. *Example.* The following example illustrates the efficiency of reflective tomography. We consider a sequence of 360 images of size 342×181 , measured by turning around the scene, one degree step (courtesy of Thales Optronique SA). These images have been recorded by a real laser system. See Figure 1 for samples of the sequence. Using a home-made software, the FDK reconstruction from these 360 images takes 2.6 seconds on a Graphics Processing Unit (Nvidia Tesla C2075). Then the reconstruction is displayed in real-time, using a volume rendering method (Maximum Intensity Projection [31]). In the Figure 2, we represent snapshots of such re-projections. The representations of the reconstruction contains clearly features and details that are useful for the recognition.

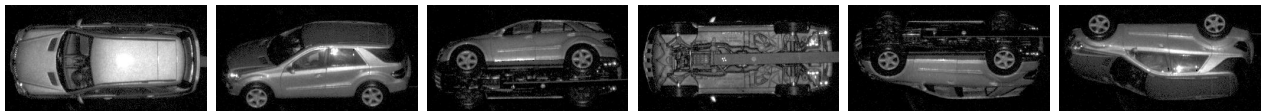


FIGURE 1. A few images of a sequence of real laser images.

1.2. **Mathematical gap.** To the authors' knowledge, reflective tomography is mainly known in optical engineering; it is still unknown in mathematical communities, whereas it introduces interesting mathematical challenges.

1.2.1. *X-ray inversion in the visible to near-infrared band.* The usual imaging methods, such as multiple-view reconstruction, shape-from-silhouette, or transmission tomography, tries to invert some forward model, to find respectively the location of features, the visual hull, or the attenuation. This is not the case for reflective tomography which is an empirical approach. This last heuristic inherits characteristics of the previous methods, without being an exact inversion procedure: it applies the inversion formula of transmission tomography, it contains a backprojection step as shape-from-silhouette, and it recovers features of the original

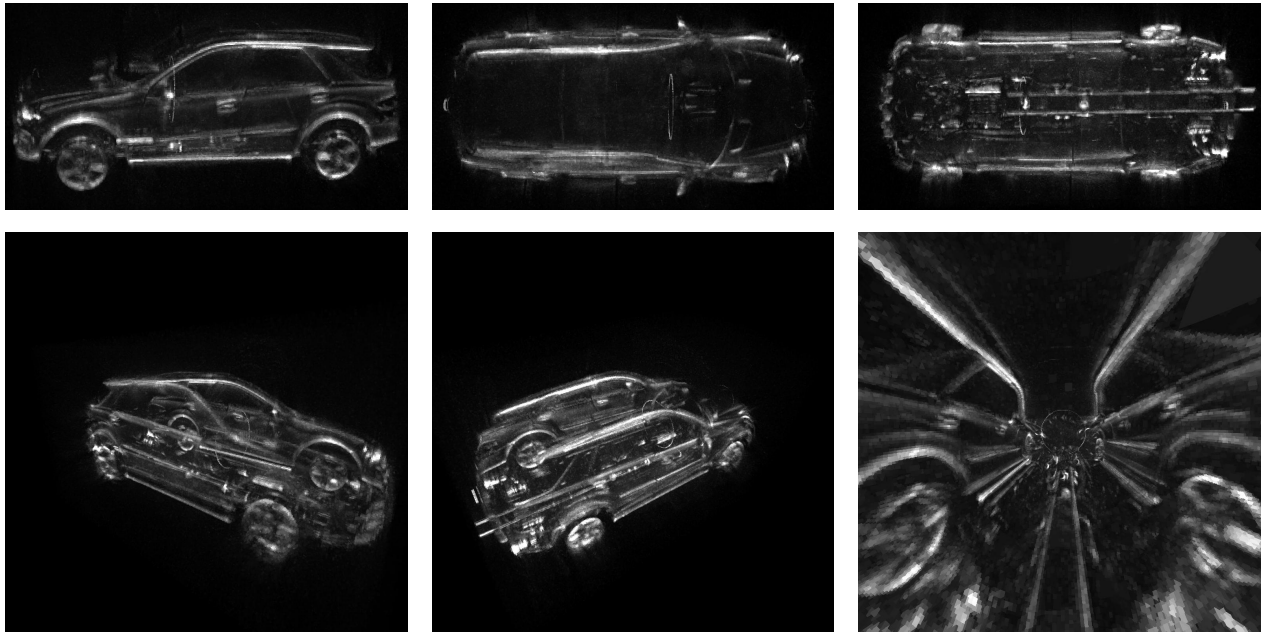


FIGURE 2. Volume rendering of a 3D tomographic reconstruction from 2D laser images.

scene as multiple-view reconstruction does. The numerical results of the previous work demonstrate that this works. But proving in a mathematical framework that this X-ray inversion of optical images in the visible to near-infrared band reconstructs the surfaces of the scene is still an open question.

1.2.2. *Radon inversion of incomplete data.* Many materials are often opaque at the considered wavelengths. This has a strong consequence. In general, a point of the scene is not visible on each plane of projection, due to occlusions: thus the data are incomplete [27]. Not only applies reflective tomography an X-ray inversion on other things than X-ray projections, but also the data are incomplete. By the way, it is known in the field of transmission tomography that serious difficulties appear for incomplete data, such as instabilities and formation of artifacts [25]. In particular, despite transmission tomography has been extensively studied over the past decades, there are still ongoing works about the Radon inversion of incomplete data: it can characterize the artifacts, and then strategies of artifact reduction can be derived [12, 16]. For that point, the problem of reflective tomography meets the trendy problem of limited Radon data. A study of reflective tomography in a well-suited framework should also be a way to describe its artifacts.

1.3. Contributions of this work.

1.3.1. *From Optics to Mathematics.* In this work, we transfer results from optical engineering to applied mathematics. We define geometric problems and a heuristic solver inspired from reflective tomography. We formulate in a proper way a geometrical version of problems that arise in this field.

We define an original class of geometric problems. For that purpose we define a new transform that we call the *reflective projection*; it encodes a geometric version of the incident irradiance on sensors in optics. The main geometric problem is to invert this transform: reconstruct the initial surfaces of a scene, from the (partial) knowledge of a reflective projection of the surfaces. In this way, we have transferred a problem from optical imaging to a problem of *geometric tomography*:

“*Geometric tomography* is the area of mathematics dealing with the retrieval of information about a geometric object from data about its sections, or projections, or both”, Gardner [17].

Furthermore, concerning the inversion of the reflective projection, we transfer the heuristic principle of reflective tomography: apply an algorithm from transmission tomography, for the right geometry of acquisition. In this way, we propose a scheme, in general linear (filtered backprojection), which solves efficiently an original non-linear geometric problem. Then the main question is to understand the result of this heuristics.

1.3.2. *Discussion about the heuristics.* We combine analytic calculations for a canonical case and numerical results in order to discuss the effect of the heuristics. Roughly speaking, this discussion reveals that the heuristics computes a volumic reconstruction, in which some features of the original surfaces are enlightened; these features come from the backprojection of the discontinuities of the data set.

The canonical case concerns the reconstruction of a sphere ∂K from its silhouettes, for a horizontal cone beam scan. We determine the exact structure of such a reflective projection: we find a surface \mathcal{S} of singularity, based on the rays of projection that are tangent to the sphere. Concerning the reconstruction, we guess, from this surface \mathcal{S} , three regimes representing respectively the noise, the useful reconstruction, and the artifacts:

- the reconstructed value should be in general low;
- the reconstructed value should be high at the points of the initial surface ∂K that are projected on a ray of \mathcal{S} ;
- the reconstructed value can be high along some lines of projection which are tangent to the surface ∂K , with a condition (that we determine) on the tangent plane.

The numerical results consider three kinds of data:

- projections with discontinuities due to the geometry or due to the projected texture;
- projections which are smoothed and thus without discontinuities;
- projections of a fluctuating texture which keep the discontinuities of the silhouettes.

The main conclusion of these tests is again that the heuristics looks essentially like a backprojection of the discontinuities of the projections, at their true location in space.

1.4. Impact of this work.

1.4.1. *In Mathematics.* This work does not aim at filling definitively the mathematical gap described in the previous section. But it introduces several ingredients for further studies. Geometric problems of interest have been defined in a proper way, and we have extended the observations of the discussion under the form of conjectures. We suggest approaches to explore this new kind of geometric problems. Proofs based on asymptotic expansions are currently under study [2], while microlocal analysis [12, 26] should be also a relevant framework: we have seen that the singularities play a central role. This work lays the foundation for more advanced studies of the subject.

By the way, geometric tomography establishes a correspondence between transmission tomography and some geometric problems [17]. In this work, this correspondence goes further: the proposed heuristics directly uses algorithms from the first class of problems to solve problems of the second class: algorithms of transmission tomography solve efficiently geometric problems! More generally we could imagine extensions of the principle to solve efficiently other geometric problems.

1.4.2. *In Optics.* The proposed geometric problems are the core of the solver in reflective tomography. Hence understanding them is important for optical applications: it is a way to strengthen the subject, and it may yield improvements of the solver, such as denoising, artifact reduction, or acceleration.

Here we have seen that the structure of the projections, especially the singularities, is more important than the values themselves. This has a strong impact: reflective tomography is very robust. It enables active/passive imagery, reconstruction of active surfaces, and so on.

1.5. **Organization.** The paper is organized as follows. In the first part, we transfer the ideas of reflective tomography from optics to geometry; in particular we propose a heuristics for problems of geometric tomography. In the second part, we examine in details the heuristics on the silhouettes of a ball. In the third part, we present several numerical tests which emphasize the impact of the discontinuities. To finish with, we formulate conjectures that must be investigated in further studies.

2. MATHEMATICAL FRAMEWORK

2.1. Geometric problems.

2.1.1. *Geometric inversion.* We represent a scene of one or several objects by a compact set $K \subset \mathbb{R}^3$. We will project such a scene along rays. An opacity constraint is taken into account using a notion of visibility:

Definition 1. A ray is a half-line $L = \{x_0 + tu, t \geq 0\}$ with $x_0 \in \mathbb{R}^3$ and $u \in \mathbb{S}^2$; L and $(x_0, u) \in \mathbb{R}^3 \times \mathbb{S}^2$ are identified.

Definition 2 (Visible point). Let $K \subset \mathbb{R}^3$ be a compact set, and let $L(x_0, u) \in \mathbb{R}^3 \times \mathbb{S}^2$ be a ray which intersects K : $L \cap K \neq \emptyset$. The *visible point* $v_K(L)$ of K along the ray L is defined by: $v_K(L) = \arg \min\{(v - x_0) \cdot u, v \in L \cap K\}$; in particular, $v_K(L) \in \partial K \cap L$. We adopt the convention that $v_K(L) = \infty$ if $K \cap L = \emptyset$.

Roughly speaking, for every ray $L(x_0, u)$, the visible point of K is the first point of K when we travel from x_0 in the direction u : see Figure 3.

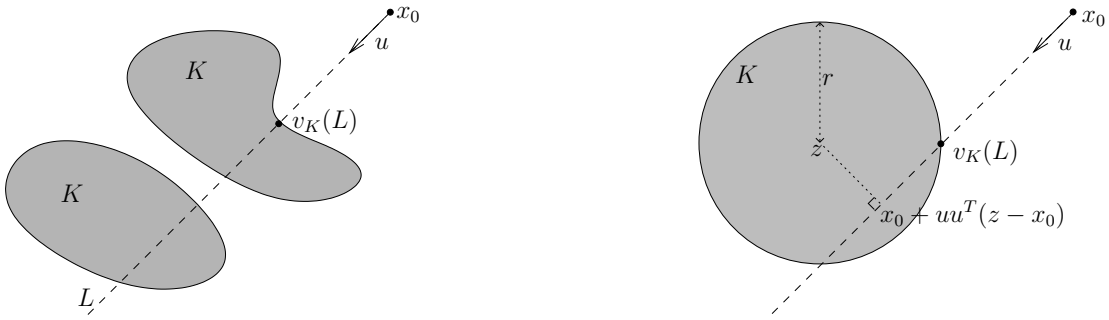


FIGURE 3. Left: visible point $v_K(L) \in \partial K \cap L(x_0, u)$. Right: $v_K(L)$ when K is the ball of radius r centered at z .

Definition 3 (Reflective projection). Let $K \subset \mathbb{R}^3$ be a compact set. Let $f : \partial K \times \mathbb{S}^2 \rightarrow \mathbb{R}$ be a function; we adopt the convention that $f(\infty, \cdot) = 0$. The *reflective projection* of f is

$$\begin{aligned} \mathcal{P}[f] : \mathbb{R}^3 \times \mathbb{S}^2 &\longrightarrow \mathbb{R} \\ L(x_0, u) &\longmapsto f(v_K(L), u). \end{aligned}$$

Remark 1. The values $\mathcal{P}[f](L)$, or more generally the restrictions of $\mathcal{P}[f]$ will be also called reflective projections.

Roughly speaking, along the ray $L(x_0, u)$, the reflective projection $\mathcal{P}[f](L) = f(v_K(L), u)$ represents an information which travels from the visible point $v_K(L)$ toward the origin x_0 , in the direction $-u$. This information depends on the visible point $v_K(L)$ but also on the direction u . If L does not meet K , $\mathcal{P}[f](L) = 0$ due to the convention. We propose now a name dedicated to graphical representations of reflective projections:

Definition 4. Let $F = \mathcal{P}[f]$ be a reflective projection. A *reflectogram* of F (or of f) is a graphical representation of F .

Such representations have peculiarities. If $v \in \partial K$, the set of rays whose visible point is v is $\{L : v_K(L) = v\}$. If we follow this set through a reflectogram of $\mathcal{P}[f]$, we observe the intensities of projection of v : $f(v, \cdot)$. In general the set $\{L : v_K(L) = v\}$ does not cross the whole reflectogram due to the definition of the visible point: occlusions appear.

We can now formulate a problem of reconstruction from a set of reflective projections:

Problem 1 (Geometric inversion of reflective projections). Let $K \subset \mathbb{R}^3$ be a compact set, $f : \partial K \times \mathbb{S}^2 \rightarrow \mathbb{R}$, and let $\mathcal{L} \subset \mathbb{R}^3 \times \mathbb{S}^2$ be a set of rays. For every $L \in \mathcal{L}$, we record the reflective projection $\mathcal{P}[f](L)$. We assume that K and f are unknown, while \mathcal{L} and $\mathcal{P}[f]|_{\mathcal{L}}$ are known. Question: reconstruct the set ∂K from $\mathcal{P}[f]|_{\mathcal{L}}$.

This problem is in general difficult. The transform of this problem:

$$\mathcal{P} : [f : \partial K \times \mathbb{S}^2 \rightarrow \mathbb{R}] \mapsto \mathcal{P}[f]|_{\mathcal{L}},$$

is in general neither invertible, nor linear. Nonetheless we will see a heuristics which can efficiently solve such a problem.

Remark 2. Similar concepts can be analogously introduced for the two-dimensional case in \mathbb{R}^2 . We use the same terminology and the same notations:

Problem (Geometric inversion of reflective projections in 2D). Let $K \subset \mathbb{R}^2$ be a compact set, $f : \partial K \times \mathbb{S}^1 \rightarrow \mathbb{R}$, and let $\mathcal{L} \subset \mathbb{R}^2 \times \mathbb{S}^1$ be a set of rays. For every $L \in \mathcal{L}$, we record the reflective projection $\mathcal{P}[f](L)$. We assume that K and f are unknown, while \mathcal{L} and $\mathcal{P}[f]|_{\mathcal{L}}$ are known. Question: reconstruct the set ∂K from $\mathcal{P}[f]|_{\mathcal{L}}$.

2.1.2. *Scanning geometries.* We now formulate two special choices for the set of rays \mathcal{L} in Problem 1. The first choice defines the cone beam scan. This case occurs when we consider a camera that turns around a scene on a circle: assuming a pinhole model for the camera, each image is a perspective projection, while the optical center scans a circle.

Definition 5 (Cone beam scan). Let $r, a, b > 0$. For every $\beta \in [0, 2\pi]$, we set: $\theta(\beta) = (\cos \beta, \sin \beta, 0)$, $\theta_{\perp}(\beta) = (\sin \beta, -\cos \beta, 0)$, $e_3 = (0, 0, 1)$, $x_0(\beta) = r\theta(\beta)$. For every $(y_{\perp}, y_3) \in [-a, a] \times [-b, b]$, we set $y = y_{\perp}\theta_{\perp}(\beta) + y_3e_3$; the unit vector that points from x_0 to $y \in \theta(\beta)^{\perp}$ is $u(\beta, y_{\perp}, y_3) = \frac{y - x_0}{|y - x_0|}$. The set of rays $\mathcal{L}_{\text{CB}}(r, a, b) = \{(x_0(\beta), u(\beta, y_{\perp}, y_3)), \beta \in [0, 2\pi], (y_{\perp}, y_3) \in [-a, a] \times [-b, b]\}$ defines the rays of a *cone beam scan*.

Here, for every β , the rays $(x_0(\beta), u(\beta, y_{\perp}, y_3)), (y_{\perp}, y_3) \in [-a, a] \times [-b, b]$, are rays of a perspective projection through $x_0(\beta)$: see Figure 4. Furthermore the optical center $x_0(\beta)$ scans the horizontal circle $\{x_1^2 + x_2^2 = r^2, x_3 = 0\}$ when β scans $[0, 2\pi]$.

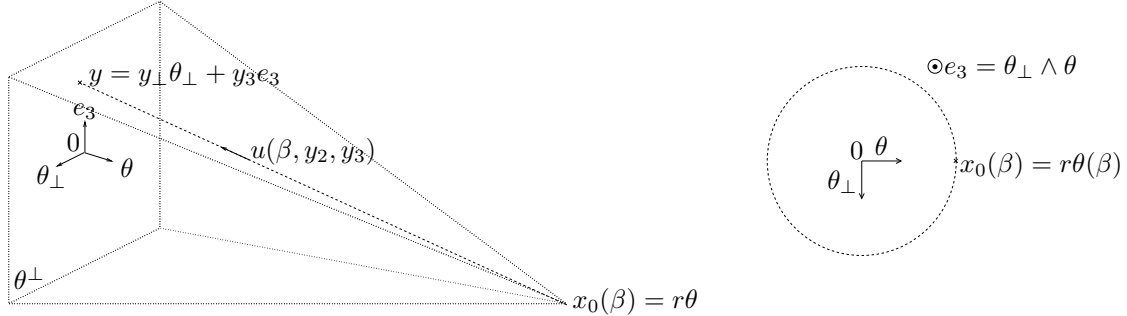


FIGURE 4. Cone beam scan: perspective rays (x_0, u) through the optical center x_0 (left); the optical center $x_0(\beta)$ scans $\{x_1^2 + x_2^2 = r^2, x_3 = 0\}$ (right).

When r becomes large compared to the size of K , the perspective projections of K look like orthographic projections along parallel rays. Then we mention a scan with orthographic projections; this is often used in order to approximate perspective projections, when the distance scene-camera is large compared to the distances in the scene.

Definition 6 (Orthographic scan). Let $r, a, b > 0$. For every $\beta \in [0, 2\pi]$, we set: $\theta(\beta) = (\cos \beta, \sin \beta, 0)$, $\theta_{\perp}(\beta) = (\sin \beta, -\cos \beta, 0)$, $e_3 = (0, 0, 1)$, $u(\beta) = -\theta(\beta)$. For every $(y_{\perp}, y_3) \in [-a, a] \times [-b, b]$, we set $x_0(\beta, y_{\perp}, y_3) = r\theta(\beta) + y_{\perp}\theta_{\perp}(\beta) + y_3e_3$. The set of rays $\mathcal{L}_{\parallel}(r, a, b) = \{(x_0(\beta, y_{\perp}, y_3), u(\beta)), \beta \in [0, 2\pi], (y_{\perp}, y_3) \in [-a, a] \times [-b, b]\}$ defines the rays of an *orthographic scan*.

Here we can see that the problem of 3D reconstruction from an orthographic scan $\mathcal{L}_{\parallel}(r, a, b)$ can be reduced to problems of 2D reconstruction from orthographic scans in 2D. Indeed, if $\mathcal{L} = \mathcal{L}_{\parallel}(r, a, b)$, the knowledge of $\mathcal{P}[f]_{\mathcal{L}}$ is equivalent to the knowledge of the horizontal cross-sections:

$$\mathcal{P}[f]_{H_{y_3}}|_{\mathcal{L} \cap H_{y_3}}, \quad H_{y_3} = \{(x, y_3), (u, 0), x \in \mathbb{R}^2, u \in \mathbb{S}^1\}, \quad y_3 \in [-b, b].$$

This motivates the problem of reconstruction from orthographic reflective projections in 2D [3].

2.2. Tomography.

2.2.1. *General formulation.* The standard model of transmission tomography is based on the X-ray transform:

Definition 7 (X-ray transform). Let $f : \mathbb{R}^3 \rightarrow \mathbb{R}$ (integrable over lines). The X-ray transform of f is:

$$\begin{aligned} \mathcal{R}[f] : \mathbb{R}^3 \times \mathbb{S}^2 &\longrightarrow \mathbb{R} \\ (x, u) &\longmapsto \int_{\mathbb{R}} f(x + tu) dt. \end{aligned}$$

Here a point v gives a contribution for every ray of the set $\{L : v \in L\}$; a graphical representation of such tomographic data is often called a *tomogram*, or a *sinogram*.

Problem 2 (Inversion of X-rays). Let $f : \mathbb{R}^3 \rightarrow \mathbb{R}$, and let $\mathcal{L} \subset \mathbb{R}^3 \times \mathbb{S}^2$ be a set of rays. For every $L \in \mathcal{L}$, we record $\mathcal{R}[f](L)$. Question: reconstruct f from $\mathcal{R}[f]_{\mathcal{L}}$.

This problem is now linear. We can find in the literature efficient reconstruction procedures, at least for some sets of rays \mathcal{L} , such as the rays of a cone beam scan, or the rays of an orthographic scan. The analogous bi-dimensional problem is the Radon inversion, which is often solved by the well-known filtered backprojection algorithm [25].

Problem 1 and Problem 2 are not the same, but the geometry of the reflective projection $\mathcal{P}[\cdot]_{\mathcal{L}}$ and the geometry of the X-ray transform $\mathcal{R}[\cdot]_{\mathcal{L}}$ have similarities: the scene is projected along the rays of \mathcal{L} . The main idea of reflective tomography is to use methods which solve Problem 2 in order to solve efficiently Problem 1:

Heuristics (Principle of reflective tomography). We consider Problem 1. We assume that \mathcal{A} is an operator which solves Problem 2 for the corresponding rays: $\mathcal{A}\mathcal{R}[\cdot]_{\mathcal{L}} \approx \mathcal{I}$ (identity). Then the volumic function $\mathcal{A}\mathcal{P}[f]_{\mathcal{L}} : \mathbb{R}^3 \rightarrow \mathbb{R}$ is an empirical representation of the original set ∂K .

The main question that arises now concerns the meaning and the description of $\mathcal{A}\mathcal{P}[f]_{\mathcal{L}}$. How does it represent the shape ∂K ?

2.2.2. *Case of a cone beam scan.* We present the specific case of a cone beam scan.

Problem (Cone Beam Computed Tomography). We measure partially the X-ray transform of $f : \mathbb{R}^3 \rightarrow \mathbb{R}$, by cone beam scanning: $\mathcal{R}[f]_{\mathcal{L}_{\text{CB}}(r, a, b)}$. Question: reconstruct f from $\mathcal{R}[f]_{\mathcal{L}_{\text{CB}}(r, a, b)}$.

The FDK algorithm presented page 8 is a very popular heuristics which solves this problem. Roughly speaking, it provides a *filtered backprojection* operator $\mathcal{A} = \mathcal{B}\Phi$ such that

$$\mathcal{B}\Phi\mathcal{R}[f]_{\mathcal{L}_{\text{CB}}(r, a, b)} \approx f, \quad f : \mathbb{R}^3 \rightarrow \mathbb{R}.$$

It is also known that if r is large, then such an operator behaves like the filtered backprojection for orthographic projections in 2D, per horizontal cross-section.

Let us consider now Problem 1 with $\mathcal{L} = \mathcal{L}_{\text{CB}}(r, a, b)$ being the rays of a cone beam scan. We measure the reflective projection $\mathcal{P}[f]_{\mathcal{L}_{\text{CB}}(r, a, b)}$ where $f : \partial K \times \mathbb{S}^2 \rightarrow \mathbb{R}$ and ∂K are unknown; we would like to recover ∂K . Following the principle of reflective tomography, we use the reconstruction operator $\mathcal{B}\Phi$ of Problem 2: the reconstructed ∂K is represented by the volumic function

$$\mathcal{B}\Phi\mathcal{P}[f]_{\mathcal{L}_{\text{CB}}(r, a, b)} : \mathbb{R}^3 \rightarrow \mathbb{R}.$$

This solves efficiently a nonlinear geometric problem with a linear operator: this can be fastly computed on Graphics Processing Units. But proving mathematically in what extent $\mathcal{B}\Phi\mathcal{P}[f]_{\mathcal{L}_{\text{CB}}(r, a, b)}$ is a true representation of the original ∂K is still an open question. We now discuss this heuristic representation.

FDK algorithm.

Input. Projection $F : \mathcal{L}_{\text{CB}}(r, a, b) \rightarrow \mathbb{R}$, measured by a cone beam scan.

Step 1.a) Compute the weighted data set F_w :

$$F_w(\beta, y_{\perp}, y_3) = w(y_{\perp}, y_3)F(x_0(\beta), u(\beta, y_{\perp}, y_3)), \quad w(y_{\perp}, y_3) = \frac{r}{(r^2 + y_{\perp}^2 + y_3^2)^{0.5}}.$$

Step 1.b) Compute the horizontal filtering ΦF :

$$\Phi F(\beta, y_{\perp}, y_3) := \mathcal{F}^{-1}(|\sigma| \hat{h}(\sigma) \mathcal{F}(F_w(\beta, y_{\perp}, y_3))(\sigma)) \quad y_3 \in [-b, b], \beta \in [0, 2\pi],$$

where $\mathcal{F}(g)(\sigma) = \int g(y_{\perp})e^{-i\sigma y_{\perp}} dy_{\perp}$ is the Fourier transform, and \hat{h} is an even windowing function with compact support.

Step 2) Compute the backprojection $\mathcal{B}\Phi F$, where \mathcal{B} is a weighted summation over lines through x :

$$\mathcal{B}G(x) = \int_0^{2\pi} \frac{r^2}{(r - x \cdot \theta)^2} G(\beta, y_{\perp}, y_3) d\beta,$$

with $y_{\perp} = \frac{rx - \theta_1}{r - x \cdot \theta}$, $y_3 = \frac{rx_3}{r - x \cdot \theta}$, $\theta = (\cos \beta, \sin \beta, 0)$.

Output. FDK reconstruction $\mathcal{B}\Phi F$.

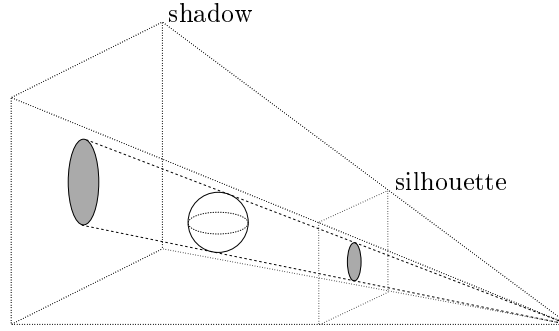


FIGURE 5. Silhouette of a ball: if K is a ball, with $f = 1$, the perspective projection $\mathcal{P}[f](x_0(\beta), u(\beta, \cdot, \cdot))$ represents a silhouette and a shadow.

3. RECONSTRUCTION FROM SILHOUETTES

3.1. Cone beam scan of a ball.

3.1.1. Reflective projection. We consider Problem 1, where: $K = \{|x - z| \leq r\}$ is the ball of radius $r > 0$ centered at $z \in \mathbb{R}^3$, $\partial K = \{|x - z| = r\}$ is the corresponding sphere, $f : (v, u) \in \partial K \times \mathbb{S}^2 \mapsto 1$ is constant, $\mathcal{L} = \mathcal{L}_{\text{CB}}(R, M, M)$ with $R, M > 0$ (large enough). In that case, the reflective projection for a fixed angle β_0 , $\mathcal{P}[f]|_{\mathcal{L} \cap \{\beta = \beta_0\}}$, represents the *silhouette*, or the *shadow*, of the object K : see Figure 5. It is clear that $\mathcal{P}[f]$ and $\mathcal{R}[\chi(K)]$ have the same support, and that $\mathcal{P}[f] = \chi(\text{supp } \mathcal{R}[\chi(K)])$, where χ is the characteristic function and supp denotes the support [17].

We use the parametrization of \mathcal{L}_{CB} (see Definition 5): a ray of the scan takes the form $L(x_0(\beta), u(\beta, y_{\perp}, y_3)) \in \mathcal{L}$, with $(\beta, y_{\perp}, y_3) \in [0, 2\pi] \times [-M, M]^2$. The projection is

$$\tilde{\mathcal{P}}[f](\beta, y_{\perp}, y_3) := \mathcal{P}[f](x_0(\beta), u(\beta, y_{\perp}, y_3)).$$

As in Figure 3 (right), $L \cap K \neq \emptyset \Leftrightarrow |x_0 - z|^2 - |(x_0 - z) \cdot u|^2 \leq r^2$; in this case, the visible point is $v_K(x_0, u) = x_0 + [(z - x_0) \cdot u - C(x_0, u)]u$ where $C(x_0, u) \geq 0$ is the unique number ≥ 0 such that $v_K(x_0, u) \in \partial K$. Let

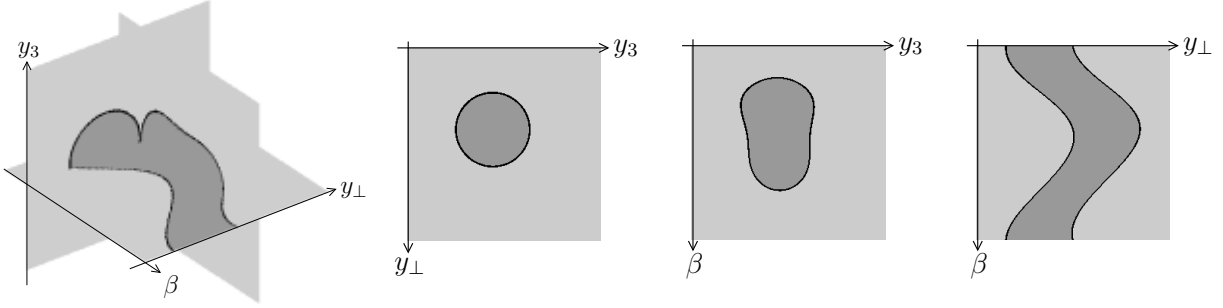


FIGURE 6. Reflectogram from silhouettes of a ball: three cross-sections of $\tilde{\mathcal{P}}[f](\beta, y_\perp, y_3)$. In light gray, $\tilde{\mathcal{P}}[f] = 0$ and $\psi > 0$, in dark gray, $\tilde{\mathcal{P}}[f] = 1$ and $\psi < 0$; in black, the interface $\psi = 0$ (or more precisely: $|\psi| < \tau$).

$\psi(\beta, y_\perp, y_3) = |x_0 - z|^2 - |(x_0 - z) \cdot u|^2 - r^2$; we get:

$$\tilde{\mathcal{P}}[f](\beta, y_\perp, y_3) = \chi(\psi^{-1}(\{t \leq 0\}))(\beta, y_\perp, y_3) = \begin{cases} 1 & \text{if } \psi(x_0, u) \leq 0, \\ 0 & \text{otherwise.} \end{cases}$$

In other words $\{\tilde{\mathcal{P}}[f] = 1\} = \{\psi \leq 0\}$, and $\{\tilde{\mathcal{P}}[f] = 0\} = \{\psi > 0\}$.

3.1.2. *Discontinuities.* The interface between these two pieces is $\mathcal{S} := \partial\{\psi \leq 0\} \cap \partial\{\psi > 0\}$. We show that $\mathcal{S} = \{\psi = 0\}$. The inclusion $\mathcal{S} \subset \{\psi = 0\}$ is due to the continuity of ψ . By the way, $\frac{\partial\psi}{\partial(y_\perp, y_3)}$ does not vanish on $\{\psi = 0\}$: by the chain rule,

$$\frac{\partial\psi}{\partial(y_\perp, y_3)} = -2[(x_0 - z) \cdot u](x_0 - z)^T \frac{\partial u}{\partial(y_\perp, y_3)}, \quad \text{with } \frac{\partial u}{\partial(y_\perp, y_3)} = \frac{1}{|y - x_0|} (I - uu^T)[\theta_\perp, e_3],$$

where $y = y_\perp \theta_\perp + y_3 e_3$, and $I - uu^T$ is the orthogonal projection on u^\perp . If R is large enough, then $(x_0 - z) \cdot u \neq 0$; so $\frac{\partial\psi}{\partial(y_\perp, y_3)} = 0 \Leftrightarrow (I - uu^T)(x_0 - z) \perp \text{span}(\theta_\perp, e_3) = \theta^\perp$. But due to the condition $\psi = 0$, $x_0 - z$ and u are linearly independent and so $(I - uu^T)(x_0 - z) \in u^\perp \setminus \{0\}$. Then

$$\frac{\partial\psi}{\partial(y_\perp, y_3)} = 0 \Leftrightarrow u \in \theta^\perp.$$

But $u \notin \theta^\perp$ and so $\frac{\partial\psi}{\partial(y_\perp, y_3)} \neq 0$. Hence the sign of ψ changes across $\{\psi = 0\}$, and then $\{\psi = 0\} \subset \partial\{\psi \leq 0\} \subset \mathcal{S}$. This also proves that the rank of the jacobian of ψ is one on \mathcal{S} . And thus \mathcal{S} is a surface.

$\tilde{\mathcal{P}}[f]$ is a piecewise constant function and its discontinuities occur at the surface \mathcal{S} . In Figure 6, we get a reflectogram of $\mathcal{P}[f]$ by the means of three cross-sections of $\tilde{\mathcal{P}}[f]$. Here we have emphasized the interface \mathcal{S} by drawing $\{|\psi| < \tau\}$ where $\tau > 0$ is a small threshold. This interface \mathcal{S} encodes the same information than $\tilde{\mathcal{P}}[f]$, so it is an object of interest. One can check that

$$\psi = 0 \Leftrightarrow x_0 + uu^T(z - x_0) \in \partial K.$$

Hence

$$\mathcal{S} = \{(\beta, y_\perp, y_3) : (x_0(\beta), u(\beta, y_\perp, y_3)) \text{ is tangent to } \partial K\}.$$

If $(\beta, y_\perp, y_3) \in \mathcal{S}$, the visible point is $v_K = x_0 + uu^T(z - x_0)$ (and $u \cdot (v_K - z) = 0$). In Figure 3 (right), it means that v_K and $x_0 + uu^T(z - x_0)$ are equal.

3.2. **Heuristic reconstruction of the sphere.** We now investigate the effect of the FDK algorithm on $\tilde{\mathcal{P}}[f]$.

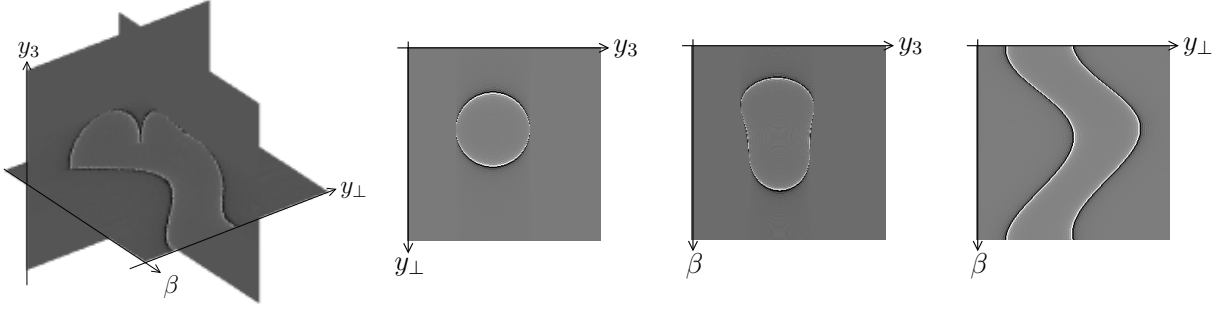


FIGURE 7. Cross-sections of the filtered projection $\Phi\mathcal{P}[f]$; the same cross-sections for $\tilde{P}[f]$ before filtering are on Figure 6.

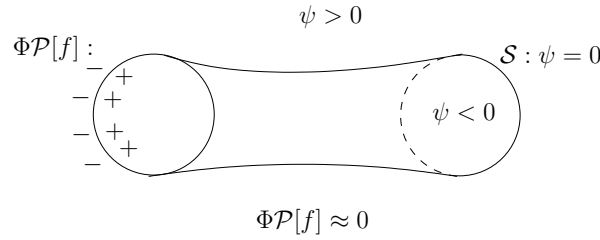


FIGURE 8. The filtered projection $\Phi\mathcal{P}[f]$ looks like a zero-crossing detection of $\mathcal{S} : \psi = 0$.

3.2.1. Filtering. The first step computes the filtered projection $\Phi\mathcal{P}[f]$: see Figure 7 for cross-sections. We observe that this step especially detects and emphasizes the singularity \mathcal{S} . The filter $\mathcal{F}^{-1}(|\sigma|\hat{h}(\sigma))(y_\perp)$ is indeed the derivative ∂_{y_\perp} , followed by a regularized Hilbert transform in y_\perp [25]. As a result, for all β and y_3 , this step emphasizes the contours of $y_\perp \mapsto \tilde{P}[f](\beta, y_\perp, y_3)$; it is a zero-crossing detection. The significant values of $\Phi\mathcal{P}[f]$ are located near the surface $\mathcal{S} : \psi = 0$ and the sign of $\Phi\mathcal{P}[f]$ is expected to change across \mathcal{S} (zero-crossing). See Figure 8.

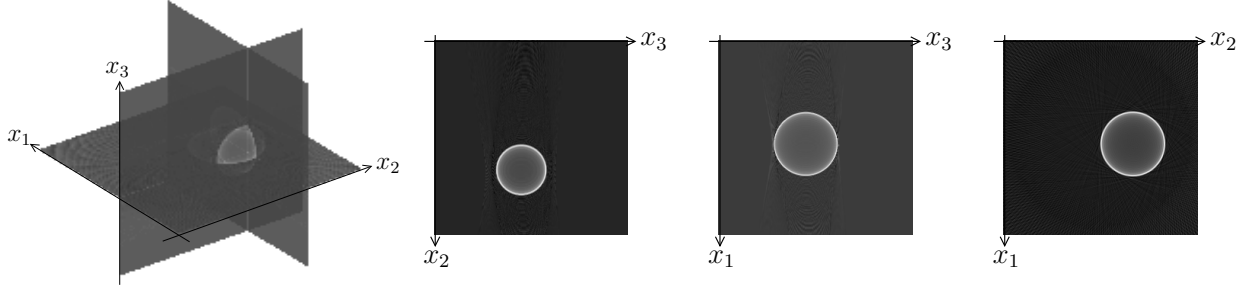
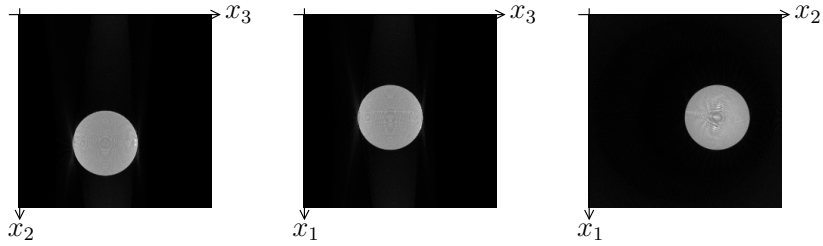
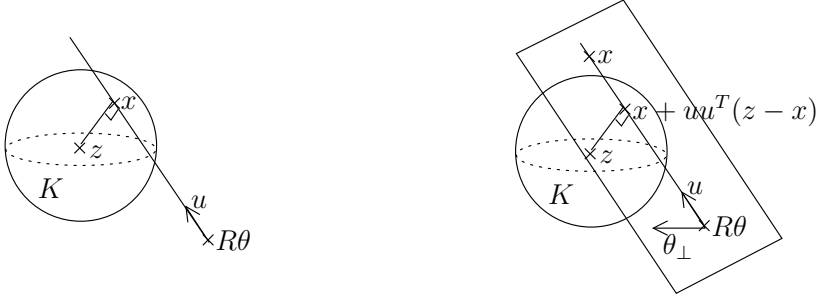
3.2.2. Backprojection. The second step computes the backprojection $\mathcal{B}\Phi\mathcal{P}[f]$; see Figure 9 for orthogonal cross-sections in this reconstruction, and Figure 10 for Maximum Intensity Projections. For every point x , the reconstruction $\mathcal{B}\Phi\mathcal{P}[f](x)$ is especially a summation through $\Phi\mathcal{P}[f]$, along the curve $\gamma(\beta) = (\beta, \hat{x}_\perp(\beta), \hat{x}_3(\beta))$, $\beta \in [0, 2\pi]$; here, $\hat{x}_\perp(\beta) = \frac{R\theta_\perp}{R-x\cdot\theta}$, $\hat{x}_3(\beta) = \frac{Rx_3}{R-x\cdot\theta}$ denotes the coordinates of the projection of x : $R\theta$, x and $\hat{x}_\perp\theta_\perp + \hat{x}_3e_3$ are aligned. In general this is a summation of arbitrary signed values. These values are small far from \mathcal{S} , but are large in a neighborhood of \mathcal{S} . The summation “cancels” the values in general. But for special circumstances, high values of the same sign are accumulated without being compensated and thus the sum is high. We want to identify such high contributions. So we study the cancellation of the function ψ along γ , by considering $\psi \circ \gamma(\beta) = |x - z|^2 - |(x - z) \cdot u|^2 - r^2$, with $u = \frac{x - R\theta}{|x - R\theta|}$.

Case a. Firstly, $\psi \circ \gamma(\beta) = 0 \Leftrightarrow x + uu^T(z - x) \in \partial K \Leftrightarrow$ the line $(R\theta, x)$ is tangent to K . In particular, if the line $(R\theta(\beta), x)$ is far from the tangents of K , then $\Phi\mathcal{P}[f](\gamma(\beta))$ is small and of arbitrary sign; it does not provide a significant value at x .

Case b. Secondly, we study the case where the line $(R\theta(\beta_0), x)$ is tangent to K , i.e. (x, β_0) is such that $\psi \circ \gamma(\beta_0) = 0$. The derivative of $\psi \circ \gamma$ is:

$$\frac{d}{d\beta}\psi \circ \gamma(\beta) = -2[(x - z) \cdot u](x - z) \cdot \frac{du}{d\beta}, \quad \frac{du}{d\beta} = \frac{1}{|x - R\theta|}(I - uu^T)R\theta_\perp.$$

Then $\frac{d}{d\beta}\psi(\gamma(\beta)) = 0 \Leftrightarrow (x - z) \cdot u = 0$ or $\theta_\perp \cdot (I - uu^T)(x - z) = 0$. Therefore $\frac{d}{d\beta}\psi \circ \gamma(\beta_0) = 0$ if, and only if, $x \in \partial K$ or the plane $R\theta(\beta_0) + \text{span}(\theta_\perp(\beta_0), u(\beta_0))$ is tangent to K . See Figure 11.


 FIGURE 9. Cross-sections of the reconstruction $\mathcal{B}\Phi\mathcal{P}[f]$ of the sphere.

 FIGURE 10. Maximum Intensity Projections of the reconstruction $\mathcal{B}\Phi\mathcal{P}[f]$ of the sphere.

 FIGURE 11. Left - case b.(2-3): the ray $(R\theta, u)$ is tangent to K at x . Right - case b.(3): the ray $(R\theta, u)$ and the plane $R\theta + \text{span}(\theta_\perp, u)$ are tangent to K at $x + uu^T(z - x)$.

- (1) If $\psi(\gamma(\beta_0)) = 0$ but the other conditions are violated, then $\frac{d}{d\beta}\psi \circ \gamma(\beta_0) \neq 0$, the sign of $\psi \circ \gamma(\beta)$ changes when β crosses β_0 , and the curve γ crosses the surface \mathcal{S} at $\gamma(\beta_0)$. In that case the (weighted) values of $\Phi\mathcal{P}[f](\gamma(\beta))$ on either side of β_0 are expected to be high but with different signs; they should offset themselves by summation, and they should not contribute significantly at x . See Figure 12 (left).
- (2) On the contrary, if $(R\theta(\beta_0), x)$ is tangent to K at $x \in \partial K$ (left of Figure 11) and $R\theta(\beta_0) + \text{span}(\theta_\perp(\beta_0), u(\beta_0))$ is not tangent to K , then the second derivative is:

$$\frac{d^2\psi \circ \gamma}{d\beta^2}\Big|_{\beta=\beta_0} = -2 \left((x - z) \cdot \frac{du}{d\beta}\Big|_{\beta=\beta_0} \right)^2 < 0.$$

So the curve γ is tangent at \mathcal{S} at the point $\gamma(\beta_0)$; furthermore $\psi \circ \gamma > 0$ in a deleted neighborhood of β_0 . In that case the (weighted) values of $\Phi\mathcal{P}[f](\gamma(\beta))$ on either side of β_0 are expected to be high but with the same sign; they should be accumulated by summation and give a significant contribution

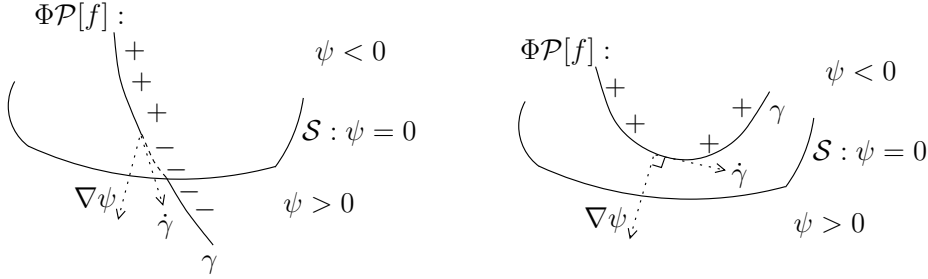


FIGURE 12. Left - case b.(1): if $\psi(\gamma(\beta_0)) = 0$ but $\frac{d\psi \circ \gamma}{d\beta}(\beta_0) \neq 0$, the values of $\Phi\mathcal{P}[f](\gamma(\beta))$ should offset themselves by summation. Right - case b.(2): if $\psi(\gamma(\beta_0)) = 0$ and $\frac{d\psi \circ \gamma}{d\beta}(\beta_0) = 0$, the values of $\Phi\mathcal{P}[f](\gamma(\beta))$ should be accumulated by summation.

at x . See Figure 12 (right). This part explains the emphasized circles (slices of the reconstructed sphere) in Figure 9.

- (3) The last case occurs when the line $(R\theta(\beta_0), x)$ and the plane $R\theta(\beta_0) + \text{span}(\theta_\perp(\beta_0), u(\beta_0))$ are tangent to K (right of Figure 11). Then $\psi \circ \gamma(\beta_0) = \frac{d}{d\beta} \psi \circ \gamma(\beta_0) = 0$ and we can expect significant contributions as before, but now along the line $(R\theta(\beta_0), x)$. This case describes eventual artifacts. Such lines are slightly remarkable in the vertical views of Figures 9 and 10.

4. NUMERICAL RESULTS

4.1. Contribution of the discontinuities. To observe the contribution of the discontinuities, we create synthetic data sets where the projected pattern f is piecewise constant with discontinuities. We increase the number of jumps from a data set to the next one.

Here, the shape ∂K is a sphere with a dent. To create this object, we deform the sphere $|x| = 1$, in spherical coordinates (ψ, φ, ρ) , where $\psi \in [-\pi, \pi]$ is the azimuth, $\varphi \in [-\frac{\pi}{2}, \frac{\pi}{2}]$ is the elevation, and $\rho > 0$ is the radius. For all points of the sphere $(\psi, \varphi, \rho = 1)$, the point of the considered surface ∂K is $(\psi, \varphi, \rho := 1 + 0.75(r - 1)\mathbb{1}_{r < 1})$, with $0.08r := (\frac{\psi}{\pi} + 1/4)^2 + (\frac{2\varphi}{\pi} + 1/6)^2$. This object is computed from a discrete version of the sphere, discretized with 640^2 patches. For all integer m , we define on this surface the following piecewise constant pattern, in spherical coordinates:

$$(\psi, \varphi) \mapsto p_m(\psi)p_m(\varphi), \quad \text{with } p_m(s) = 0.5 + 0.25\mathbb{1}_{(ms - \lfloor ms \rfloor) < 0.5}.$$

We project this pattern: for each ray $L(x_0, u)$, the projection is

$$\mathcal{P}[f](L) = f(v_K, u) := p_m(\psi)p_m(\varphi),$$

where (ψ, φ, ρ) are the spherical coordinates of the visible point $v_K \in \partial K$. We simulate an orthographic scan of this reflective projection, using plots of surfaces with `Matlab`. We consider a uniform discretization (constant steps) of size $801 \times 201 \times 201$, 801 being the number of angles of projection, and 201×201 being the size of each image.

Increasing m increases the number of jumps; we simulate data sets for several values of m : 0, 1, 2, 4, 8 and 16. On the first line of Figure 13, we represent one image of the sequence, for the successive values of m . Of course we distinguish here two kinds of jumps in the images: jumps due to discontinuities of the pattern f , and geometrical jumps due to the shape (interface object/background).

We apply the heuristics on these data sets. For the visualization, the reconstructions are re-projected, using a Maximum Intensity Projection (MIP). In order to improve the visual perception of the dent, we restrict the domain to a half-space before visualization: our full volume being a set of voxels $(i, j, k) \in [1, 201]^3$, we keep only the $j \geq 91$. On the second line of Figure 13, we represent a vertical view of the reconstructions, associated with the view of the data sets. More jumps in the input can improve the visual perception of the object, for both the input and the output. The heuristics computes much more than just a convex hull. A remarkable property here is that the dent is even more perceptible in the reconstruction than in

the reflectogram. This is because the boundary $(\frac{\psi}{\pi} + 1/4)^2 + (\frac{2\varphi}{\pi} + 1/6)^2 = 0.08$ of the dent introduces geometrical jumps in many input images; the heuristics combines them, and so the boundary is emphasized in the reconstruction.

4.2. Contribution of the smooth variations. Realistic images of realistic scenes have often jumps and smooth variations. Here we would like to observe the contribution of the smooth variations alone, and to observe what happens without discontinuities. So we create synthetic data sets whose images are smooth, and whose *frequency* increases from a data set to the next one.

We consider the sphere $\partial K : |x| = 1$, which is discretized using 640^2 patches as before. We project a smooth pattern, given in spherical coordinates by:

$$(\psi, \varphi) \mapsto 1 + 0.5 \cos m(\psi + \varphi),$$

with $m = 2^i, 1 \leq i \leq 6$, playing the role of a fixed frequency. As before, by rotating over 360 degrees, we simulate an orthographic scan of size $801 \times 201 \times 201$. The simulated images are smooth, except at the interface object/background where discontinuities occur. For the purpose of this subsection, we weight the data in order to obtain smooth images. For a pixel $(i, j) \in [1, 201] \times [1, 201]$, the weight is $(r+1)^2(r-1)^2 \mathbb{1}_{r < 1}$, with $99r(i, j) = ((i-100)^2 + (j-100)^2)^{0.5}$. On the first line of Figure 14, we represent one smooth image of the sequence that we get, for the successive values of m .

We apply the heuristics on these data sets. On the second line of Figure 14, we represent a vertical view (MIP) of the reconstructions, associated with the view of the data sets. From the visual point of view, it is easier to identify the original sphere for large m . For smooth data, the result of the heuristic may be poor for low frequency components, but is meaningful when the frequency is large enough. In any case, smooth variations in the input produce contributions which add contrasts in the renderings; they can be useful for the visual perception. The results also emphasize the importance of singularities: here, we have seen that without the discontinuities at the interface object/background in the projections, it is more difficult to reconstruct the shape.

4.3. Test of robustness. We show how the method deals with changes in the forward problem during the acquisition, by considering a randomized fluctuating pattern. This pattern could represent active surfaces whose reflectance properties are random.

For all $\sigma = 0, 2^j, -2 \leq j \leq 2$, we consider an orthographic scan $F_\sigma(\beta, y_\perp, y_3)$ of the Stanford Bunny ∂K [29]; the size of this scan is $801 \times 200 \times 157$. For each ray of projection (x_0, u) such that the angle of projection is β (and thus $u = (-\cos \beta, -\sin \beta, 0)$, see Definition 6), the projected surfacic pattern is:

$$f_\sigma(v, u) = 1 + (0.2 + \sigma \eta_1(\beta)) \sin(\pi \sigma \eta_2(\beta) + 20\pi |v|), \quad v \in \partial K,$$

where the $\eta_i(\beta)$ are independent realizations of the Gaussian $\mathcal{N}(0, 1)$. The $\sigma \eta_i(\beta)$ correspond to some modifications of the amplitude and the phase of the pattern. Increasing σ increases the dependency in β for the projected pattern. If $v \in \partial K$ is a fixed point, then along the set of rays that sees v , *i.e.* $\{(\beta, y_\perp, y_3) : v_K(x_0, u) = v\}$, the intensity level of v randomly varies with a standard deviation which increases when σ increases. To observe this, see the first line of Figure 15, where we represent reflectograms: horizontal slice $y_3 = 0$ in the reflective projections.

We apply the heuristics on these data sets. On the second line of Figure 15, we represent a vertical view of the reconstructions (MIP). Despite changes in the forward problem, the silhouette of the object still appears under the form of discontinuities in the reflective projection. As a result the heuristics successfully reconstructs the shape. By the way, the jumps at the discontinuities do not have the same values. Thus the reconstruction is better than the shape alone: surfacic contrasts are perceived. This is even true for large disturbances: see the last case, where the level of disturbance is about 4 times the intensity level of the original signal.

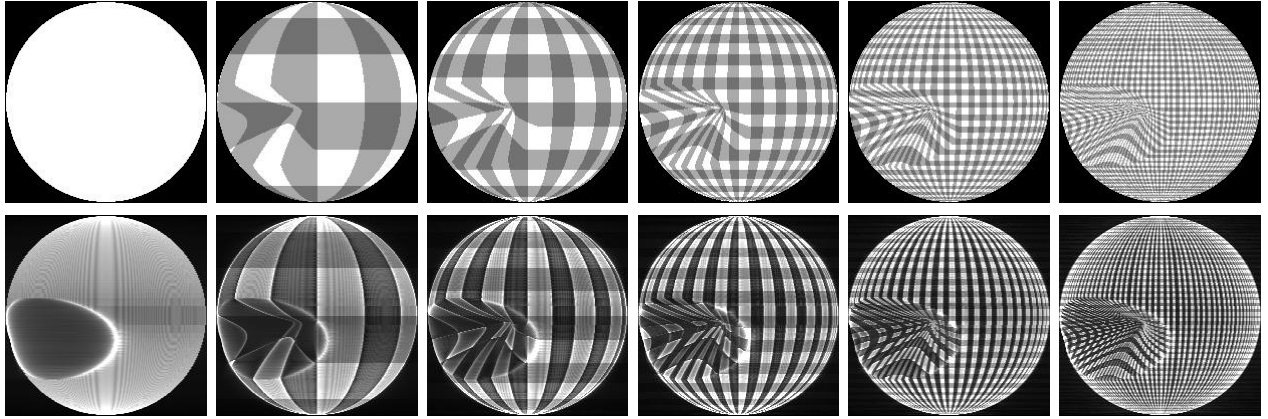


FIGURE 13. Effect of jumps for a sphere with a dent. From the left to the right: the projected pattern has more and more discontinuities, $m = 0, 2^i, 0 \leq i \leq 4$. On the first line: one image of the sequence; on the second line: associated heuristic reconstruction.

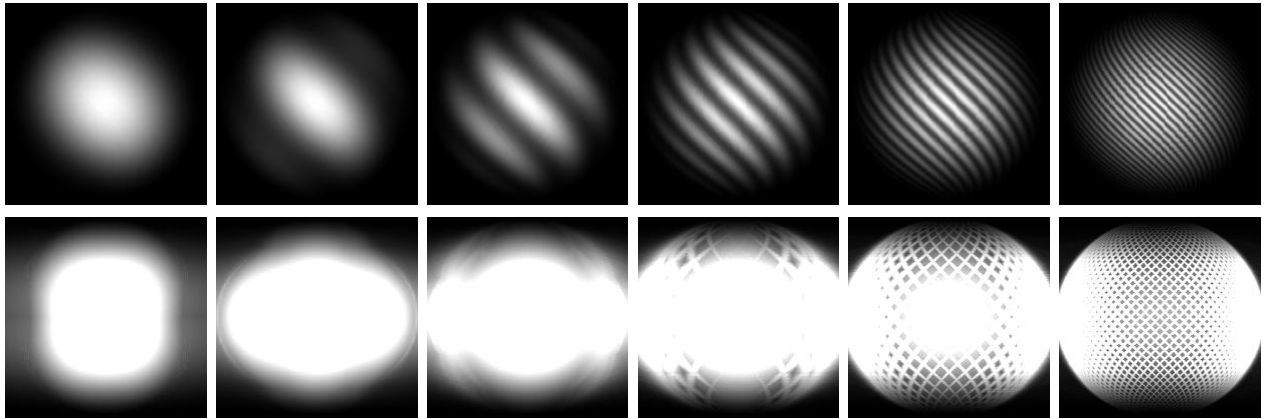


FIGURE 14. Effect of smooth variations for a sphere. From the left to the right: the frequency parameter is larger and larger: $m = 2^i, 1 \leq i \leq 6$. On the first line: one image of the sequence; on the second line: associated heuristic reconstruction.

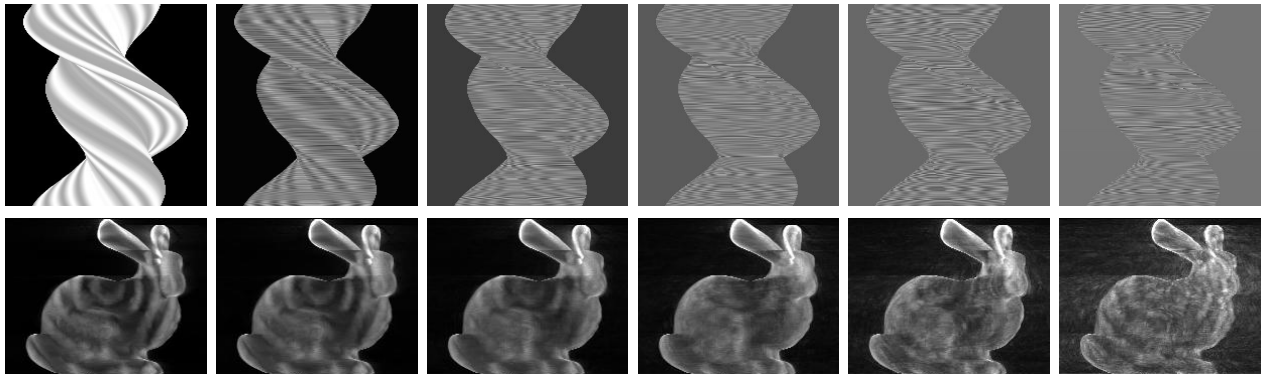


FIGURE 15. Test of robustness: from the left to the right, the level of disturbance is $\sigma = 0, 2^j, -2 \leq j \leq 2$. On the first line, reflectograms $(\beta, y_\perp) \mapsto F_\sigma(\beta, y_\perp, 0)$. On the second line: a vertical view computed by the heuristics.

5. CONJECTURES

We would like to extend the previous discussions to more general configurations. The first thing to do is to find a framework which describes the structure of a reflective projection, and more particularly its singularities. The following conjecture deals with an extension for several smooth convex objects:

Conjecture 1. *Let $(K_i)_{1 \leq i \leq N}$ be a family of compact sets such that $\overline{K_i} = K_i$ and $K_i \cap K_j = \emptyset$ if $i \neq j$. Let $(f_i)_{1 \leq i \leq N}$ be a family of distinct numbers. We assume that the K_i are convex and smooth. Let $K = \cup_{i=1}^N K_i$, and let $f : \partial K \times \mathbb{S}^2 \rightarrow \mathbb{R}$, such that $f|_{\partial K_i} = f_i, 1 \leq i \leq N$. Let $M, R > 0$ be large enough. We conjecture that the reflective projection $\mathcal{P}[f]|_{\mathcal{L}_{CB}(R, M, M)}$ is piecewise constant. We conjecture that its singularities are included in the set of the rays of $\mathcal{L}_{CB}(R, M, M)$ that are tangent to one of the K_i 's (at least), and that they describe pieces of surfaces.*

The next step is to understand the effect of the heuristics. The following conjecture states that the method is based on the singularities of the data set:

Conjecture 2. *Let $F = \mathcal{P}[f]|_{\mathcal{L}_{CB}(R, M, M)}$ be a cone-beam scan of the reflective projection of $f : \partial K \times \mathbb{S}^2 \rightarrow \mathbb{R}$. We assume that F is piecewise smooth. Let $\mathcal{S} \subset \mathcal{L}_{CB}(R, M, M)$ denotes the set of rays $L \in \mathcal{L}_{CB}(R, M, M)$ such that F is singular at L . We conjecture that the FDK reconstruction $\mathcal{B}\Phi F$ emphasizes several points, including the points $v_K(L) \in \partial K, L \in \mathcal{S}$, which are the visible points at the singularities.*

The meaning of *emphasize* must be precised. Essentially we have seen that the method consists in ‘‘accumulating coherent information’’, and in ‘‘cancelling incoherent one’’. We know that methods of stationary phase provide a mathematical framework to describe such phenomena. This option is explored in ongoing works: [2] focuses on asymptotic expansions with respect to the cut-off frequency of the filtering (width of the spectral windowing). Another idea is to study the problem in a framework of microlocal analysis: describe the singularities of the reflective projection and the singularities of the empirical reconstruction.

Such studies will strengthen the heuristics by proving what it exactly does. In particular a full description of the *emphasized* points will also describe the artifacts: the emphasized points that do not belong to ∂K . We see here that the subject meets again the problems of Radon inversion, where such ideas are currently developed to describe and reduce incompleteness artifacts [12].

REFERENCES

- [1] B.G. Baumgart. *Geometric modeling for computer vision*. PhD thesis, Stanford Univ Ca Dept of Computer Science, 1974.
- [2] J.-B. Bellet. Analyse asymptotique et géométrique de la tomographie réflective. <hal-01571707>, 2017.
- [3] J.-B. Bellet and G. Berginc. Reflective filtered backprojection. *Comptes rendus - Mathématique*, 354:960–964, 2016.
- [4] I. Berechet, G. Berginc, and S. Berechet. Method for 3D reconstruction of an object in a scene. United States Patent, No US 2013/0100131 A1, April 2013.
- [5] S. Berechet, I. Berechet, J.-B. Bellet, and G. Berginc. Procédé de discrimination et d’identification par imagerie 3D d’objets d’une scène. Patent WO2016097168 A1, 2015.
- [6] G. Berginc. Scattering models for range profiling and 2D-3D laser imagery. In Leonard M. Hanssen, editor, *Reflection, Scattering, and Diffraction from Surfaces IV, 92050K*, volume 9205 of *Proc. of SPIE*, 2014.
- [7] G. Berginc, J.-B. Bellet, I. Berechet, and S. Berechet. Optical 3D imaging and visualization of concealed objects. In *Proc. SPIE*, volume 9961, page 99610Q, 2016.
- [8] G. Berginc and M. Jouffroy. Optronic system and method dedicated to identification for formulating three-dimensional images. US patent 20110254924 A1, European patent 2333481 A1, FR 09 05720 B1, November 2009.
- [9] G. Berginc and M. Jouffroy. Simulation of 3D laser systems. In *Geoscience and Remote Sensing Symposium, 2009 IEEE International, IGARSS 2009*, volume 2, pages 440–444. IEEE, 2009.
- [10] G. Berginc and M. Jouffroy. Simulation of 3D laser imaging. *PIERS Online*, 6(5):415–419, 2010.
- [11] G. Berginc and M. Jouffroy. 3D laser imaging. *PIERS Online*, 7(5):411–415, 2011.
- [12] L. Borg, J. Friel, J.S. Jørgensen, and E.T. Quinto. Full Characterization of Reconstruction Artifacts from Arbitrary Incomplete X-ray CT Data. arXiv:1707.03055v3, 2018.
- [13] R.A. Chipman. *Polarimetry, chapter 22 in: Handbook of optics, Vol. 2: Devices, Measurements, and Properties*. McGRAW-HILL, 1994.
- [14] L.A. Feldkamp, L.C. Davis, and J.W. Kress. Practical cone-beam algorithm. *JOSA A*, 1(6):612–619, 1984.
- [15] D.S. Flynn and C. Alexander. Polarized surface scattering expressed in terms of a bidirectional reflectance distribution function matrix. *Optical engineering*, 34(6):1646–1651, 1995.

- [16] J. Friel and E.T. Quinto. Characterization and reduction of artifacts in limited angle tomography. *Inverse Problems*, 29(12):125007, 2013.
- [17] R. J. Gardner. Geometric tomography. *Notices Amer. Math. Soc.* 42, 4:422–429, 1995.
- [18] D.T. Gering and W.M. Wells. Object modeling using tomography and photography. In *Multi-View Modeling and Analysis of Visual Scenes, 1999.(MVIEW'99) Proceedings. IEEE Workshop on*, pages 11–18. IEEE, 1999.
- [19] B. Horn. *Robot vision*. MIT press, 1986.
- [20] F.K. Knight, S.R. Kulkarni, R.M. Marino, and J.K. Parker. Tomographic Techniques Applied to Laser Radar Reflective Measurements. *Lincoln Laboratory Journal*, 2(2):143–160, 1989.
- [21] K.N. Kutulakos and S.M. Seitz. A theory of shape by space carving. *International journal of computer vision*, 38(3):199–218, 2000.
- [22] A. Laurentini. The visual hull concept for silhouette-based image understanding. *IEEE Transactions on pattern analysis and machine intelligence*, 16(2):150–162, 1994.
- [23] Y. Ma, S. Soatto, J. Kosecka, and S.S. Sastry. *An invitation to 3-D vision: from images to geometric models*, volume 26. Springer Science & Business Media, 2012.
- [24] A. Mohammad-Djafari. *Problèmes inverses en imagerie et en vision (Traité Signal et Image, IC2)*. Lavoisier, 2009.
- [25] F. Natterer and F. Wübbeling. *Mathematical methods in image reconstruction*. SIAM, 2001.
- [26] A.G. Ramm and A.I. Zaslavsky. Reconstructing singularities of a function from its Radon transform. *Mathematical and computer modelling*, 18(1):109–138, 1993.
- [27] G. Rigaud, J.-B. Bellet, G. Berginc, I. Berechet, and S. Berechet. Reflective Imaging Solved by the Radon Transform. *IEEE Geoscience and Remote Sensing Letters*, 13:936–938, 2016.
- [28] J.R. II Shell. *Polarimetric remote sensing in the visible to near infrared*. PhD thesis, Rochester Institute of Technology, 2005.
- [29] G. Turk and M. Levoy. Zippered polygon meshes from range images. In *Proceedings of the 21st annual conference on Computer graphics and interactive techniques*, pages 311–318. ACM, 1994.
- [30] A.G. Voronovich. *Wave Scattering from Rough Surfaces*. Springer, 2012.
- [31] J.W. Wallis and T.R. Miller. Three-Dimensional Display in Nuclear Medicine and Radiology. *The Journal of Nuclear Medicine*, pages 534–546, 1991.
- [32] A. Yezzi and S. Soatto. Stereoscopic segmentation. *International Journal of Computer Vision*, 53(1):31–43, Jun 2003.
- [33] H. Zheng, Z. Chen, Y. Kang, and J. Liu. A New Heuristic Weighting Function for FDK-based reconstruction of Cone Beam Tomography. In Y. Peng and X. Weng, editors, *7th Asian-Pacific Conference on Medical and Biological Engineering*, pages 206–209, Berlin, Heidelberg, 2008. Springer Berlin Heidelberg.

UNIVERSITÉ DE LORRAINE, CNRS, IECL, F-57000 METZ, FRANCE
 E-mail address: jean-baptiste.bellet@univ-lorraine.fr

THALES OPTRONIQUE, 2 AVENUE GAY LUSSAC, CS 90502, 78995 ÉLANCOURT CEDEX, FRANCE
 E-mail address: gerard.berginc@fr.thalesgroup.com